Cutoff Lows Over Southwestern South America



Roberto Rondanelli, University of Chile Department of Geophysics

https://doi.org/10.1093/acrefore/9780190228620.013.976

Published online: 16 April 2025

Summary

Cutoff lows are upper level cold-core cyclones that become detached from the mid-latitude westerlies, drifting slowly toward lower latitudes. In southwestern South America, they frequently appear near 30°S and play a significant role in driving rainfall, sometimes bringing intense precipitation to areas that are normally very dry. Because these systems are often convective and move slowly, forecasting their precipitation remains challenging, yet they are a major cause of extreme rainfall and floods in northern and central Chile.

Despite their frequent occurrence, many of these storms fail to produce heavy rainfall unless they tap into sufficient moisture. A recurring factor in major flood events is the presence of a coastally trapped moisture plume that pushes water vapor southward from warmer waters near the Peru-Chile border. When these plumes intersect the topography of the Andes, the resulting uplift can trigger deep convection, causing significant precipitation and sometimes devastating floods and landslides.

Looking ahead, changing climatic conditions, including increases in sea surface temperature and atmospheric moisture, may affect both the frequency and the intensity of cutoff lows. Even moderate cyclonic disturbances can lead to major precipitation extremes when ample moisture is available. As a result, understanding the interplay between large-scale dynamics, moisture supply, and mountain uplift is crucial to improve rainfall forecasts and anticipating the impacts of future storms on one of the driest regions on Earth.

Keywords: cutoff lows, Rossby wave breaking, Atacama Desert, orographic precipitation, moisture transport, upper level cyclones, extreme rainfall, climate change

Subjects: Hydrological Cycle, Climate Systems and Climate Dynamics, Climate Impact: Extreme Events

Introduction

Cutoff lows have only been recognized as an important feature of the synoptic meteorology of southwestern South America during the early 21st century (Pizarro & Montecinos, 2000). For example, more than 50% of the precipitation in the hyper-arid core of the Atacama and its surroundings can be explained by cutoff lows (Aceituno et al., 2021). In fact, some major extreme rainfall events in the region between 20°S and 35°S are associated with cutoff lows (Bozkurt et al., 2016; Muñoz & Schultz, 2021). Some historical accounts from the 19th century seem to confirm that cutoff lows have, from time to time, produced rainfall in arid and semi-arid northern Chile. Vicuña-Mackenna (1877, pp. 453–454) refers to a storm in July 1877:

But what constitutes the most remarkable peculiarity of the rainstorm on July 10 in Atacama is not that it rained in these regions when in the south it had completely cleared, nor that each of its rain showers lasted more than twelve hours, but that its movement was reversed, from north to south, as if its generating nucleus had been in the desert, that is, in latitudes where it never rains.

The Atacama flood of 2015 is perhaps the most extreme modern example of these storms. During March 24 and 25, 2015, a cutoff low caused significant damage and tens of deaths in hyper-arid northern Chile (the blueish region in Figure 1), due to landslides and major flooding experienced in all basins of the region (Barrett et al., 2016; Bozkurt et al., 2016; Reboita & Veiga, 2017; Wilcox et al., 2016). This has led to renewed interest in understanding the physical and dynamical characteristics of cutoff lows in this region, as well as exploring changes in frequency and intensity during historical and past periods (e.g., Reyers & Shao, 2019). Not only is understanding the processes that control the existence of the driest desert on Earth interesting, but understanding how these processes can break under current climatic conditions is also interesting. Considering that climate projections for the 21st century include a robust signal of moistening along northwestern South America (e.g., Belmadani et al., 2014; Oerder et al., 2015), understanding the interaction of cutoff lows and atmospheric water vapor sources has become a major research priority.

Dynamical Features

Cutoff lows are closed cyclonic circulation in the mid- and upper levels of the troposphere that have been segregated from the mean westerly flow toward the equator (Palmén, 1949). This segregation from the mid-latitude storm track makes cutoff lows more likely to impact lower latitudes than usual baroclinic disturbances. Cutoff lows also tend to drift slowly westward because of the absence of a strong background mean flow. They are a cold-core vortex (as opposed to hurricanes, which have a warm core), and this explains some of the names they receive in Spanish, such as *gota fría* (cold droplet) or *núcleo frío en altura* (upper level cold core). Although cutoff lows are a relatively common feature of the synoptic meteorology of southwestern South America, their impacts, especially with respect to precipitation, remain challenging to forecast mainly due to the convective nature of rainfall in these episodes.

We illustrate several aspects of the typical development of cutoff lows in the southwestern Pacific using a case study of a cutoff low during April 2024. This particular cutoff low produced rainfall over central and northern Chile during the period between April 12 and 15. This cutoff low can be considered representative of precipitating cutoff lows during fall in northern Chile. Although not an extreme case, as seen in Figure 1b, this particular event was able to produce rainfall in many arid and hyper–arid regions. Some stations recorded nearly 40 mm of accumulated rainfall during this event, competing with the annual accumulation in some cases.

Potential Vorticity View

From a large-scale perspective, cutoff lows can be thought of as disturbances that originate from the polar reservoir of planetary cyclonic vorticity as a result of the Rossby wave breaking along the polar front. The Ertel-Rossby potential vorticity (PV) on an isentropic surface (e.g., McIntyre, 2003) is defined as

$$PV = -g(\zeta_{ heta} + f) rac{\partial heta}{\partial p},$$
 (1)

where g is gravity, ζ_{θ} is the relative vorticity on an isentropic surface, f is the planetary vorticity, and θ is the potential temperature.

Given that PV is materially conserved on an isentropic surface in the absence of friction and diabatic processes, cutoff lows appear as blobs of cyclonic vorticity abandoning the polar reservoir when seen in a PV map on an isentropic surface (Hoskins et al., 1985). Figure 2 shows one such case using isentropic maps on the 330-K surface from the period between April 11 and April 17, 2024. On April 11, a strong anticyclone centered around 105°W advected polar PV toward lower latitudes at around 90°W (Figure 2a). At this point, a large region at the mid-latitudes showed a reversed gradient of PV (i.e., more negative values toward the equator), between 90° and 50°W (Figure 2a–b), which is the telltale sign of a Rossby wave-breaking event. According to Ndarana and Waugh (2010), about 90% of the cases of cutoff low formation occur associated with the breaking of Rossby waves in the southern hemisphere. The low values of PV associated with the anticyclone reach approximately 60°S, and the intrusion of cyclonic PV into the subtropics continues to amplify. The original cyclonic PV trough, which gave origin to the cutoff low, has now advanced eastward and is located at about 40°W (Figure 2c).

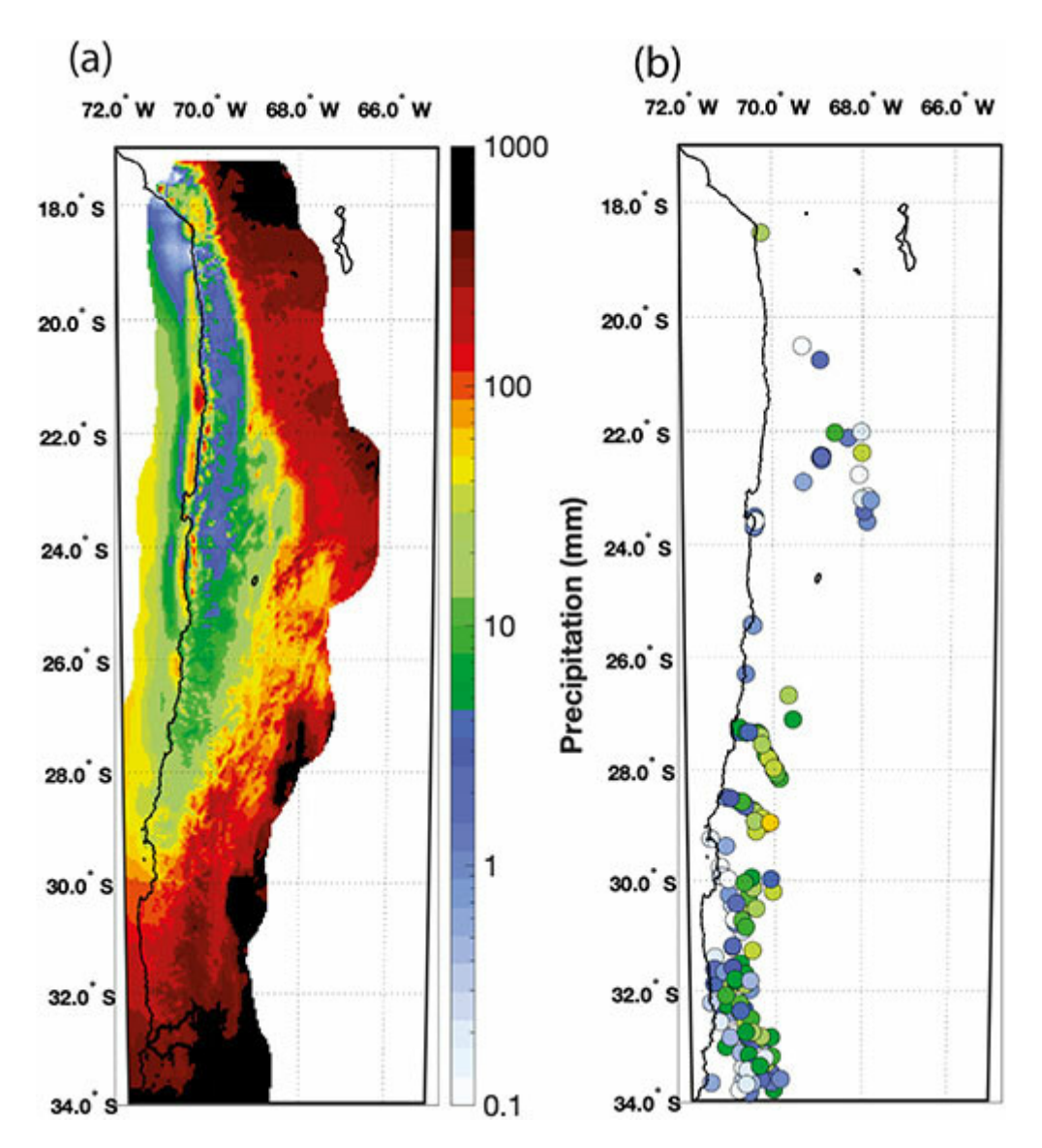


Figure 1. (a) Climatology of annual precipitation from CR2Met product. (b) Accumulated rainfall from April 12 to April 15, 2024, from surface rain gauges.

Source: (a) Boisier (2023); Boisier et al. (2018) (b) Data from vismet.cr2.cl.

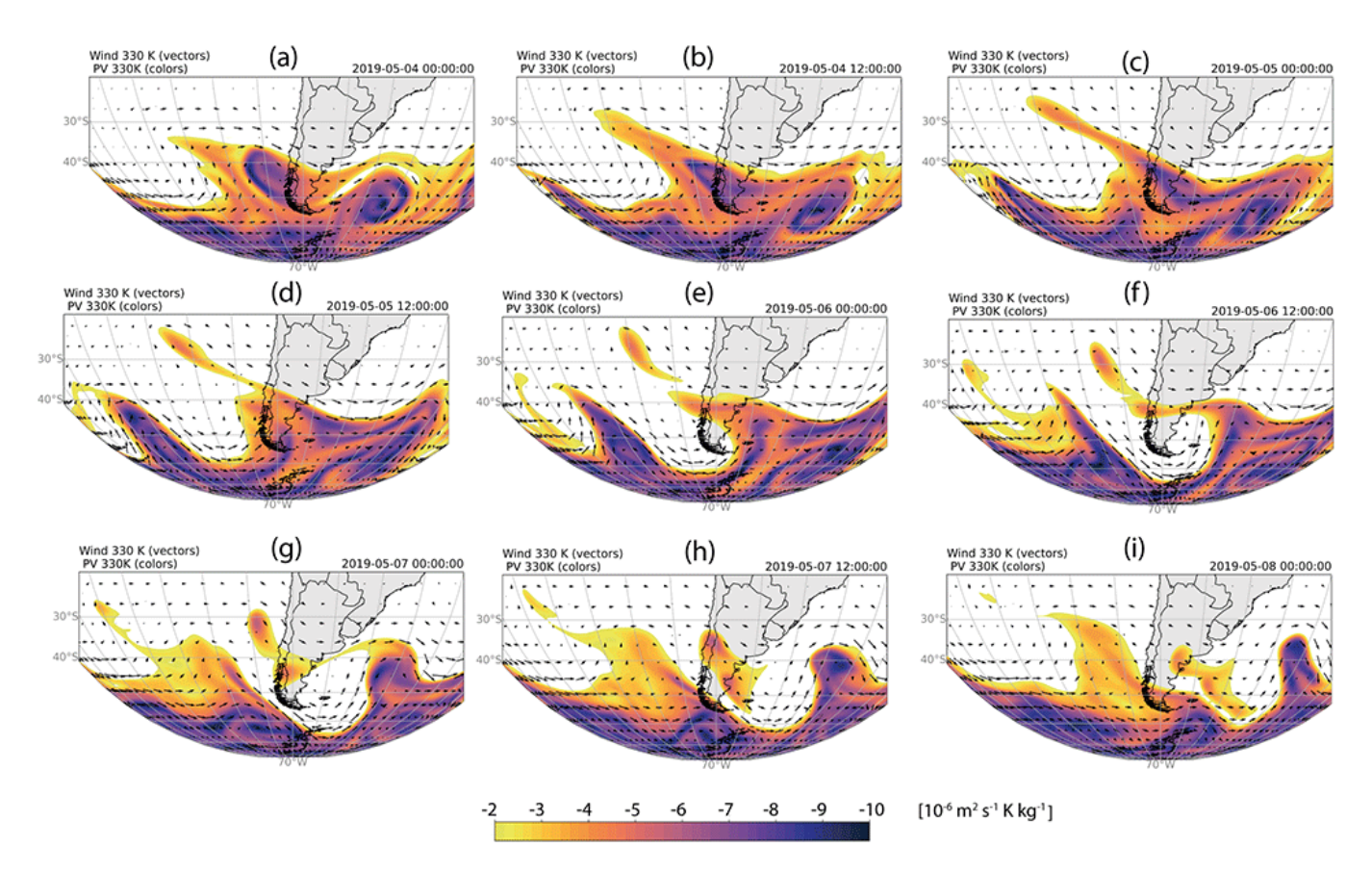


Figure 2. Isentropic potential vorticity maps from the period April 11 to April 17, 2024. Potential vorticity (PV) is in colors, and wind is in vectors over the 330-K isentropic surface.

Source: Data are from ERA5 re-analysis.

As the wave continues to amplify, it can be observed that the region connecting the main cyclonic circulation in the subtropics (centered approximately 80°W, 35°S in Figure 2d) becomes elongated and thinner. During the following 24 hours, the main cyclonic PV blob remains almost completely stationary off the coast, a feature typical of other cases. For instance, Godoy et al. (2011) show that the so-called stagnation of the cutoff low windward of the Andes occurs associated with a balance between the divergence and the horizontal vorticity advection terms of the vorticity equation. By April 14, 00 UTC, a filament is clearly visible along 45°S (Figure 2f), connecting the cutoff low to the original source of cyclonic PV, which has shifted to 30°W by this time. As the filament becomes thinner, it begins to erode due to diabatic and frictional processes (e.g., Appenzeller et al., 1996), effectively isolating the cutoff low from its polar PV reservoir (Figure 2i). An interesting example of these irreversible processes can be seen immediately before the filament breaks on April 15, 00 UTC (Figure 2h). The vorticity filament develops ellipsoidal vorticity centers similar to those found in the barotropic instability (see, e.g., Figure 3a, Appenzeller et al., 1996, and references therein). In fact, the wavelength of this feature is about 1,000 km, which, using the Rayleigh relation between the width of the vorticity region δ and the most unstable wavelength of the barotropic instability $\lambda \sim 8\delta$ (e.g., Reinaud, 2020), suggests a vorticity region width of about 135 km, closely matching the observed width of the filament. Also, the water vapor image at the same time confirms the existence of the barotropic instability in the observations, where the dry region in the image bears a striking resemblance to the solution of the non-linear barotropic equation for a parallel shear flow (see, e.g.,

Figure 6.6 in Vallis, 2006). As the vortices grow at the expense of the horizontal shear of the flow—which is the source of the vertical vorticity of the filament—turbulence and irreversible mixing will develop (Figure 2i). Between April 15, 12:00, and April 16, 00:00, (Figure 2i–j), the cutoff low crosses the Andes, losing part of its original intensity but conserving its shape. Once the cutoff low crosses the Andes, the system can tap water vapor from the Atlantic and the Amazon, and sometimes a rapid intensification of the storms associated with the system, resulting in the demise of the upper level cyclone due to diabatic heating, although in other cases the cutoff low can be intensified by the interaction with the stationary trough induced by the Andes and give rise to baroclinic development Funatsu et al. (2004). In this case, a rapid disintegration of the PV blob east of the Andes is seen (Figure 2k). Finally, the remains of cyclonic PV near the La Plata basin begin to be mixed with PV of a subsequent wave breaking. In addition, a new meridional PV feature near 100°W appears to form a new wave breaking in the Pacific (Figure 2l)

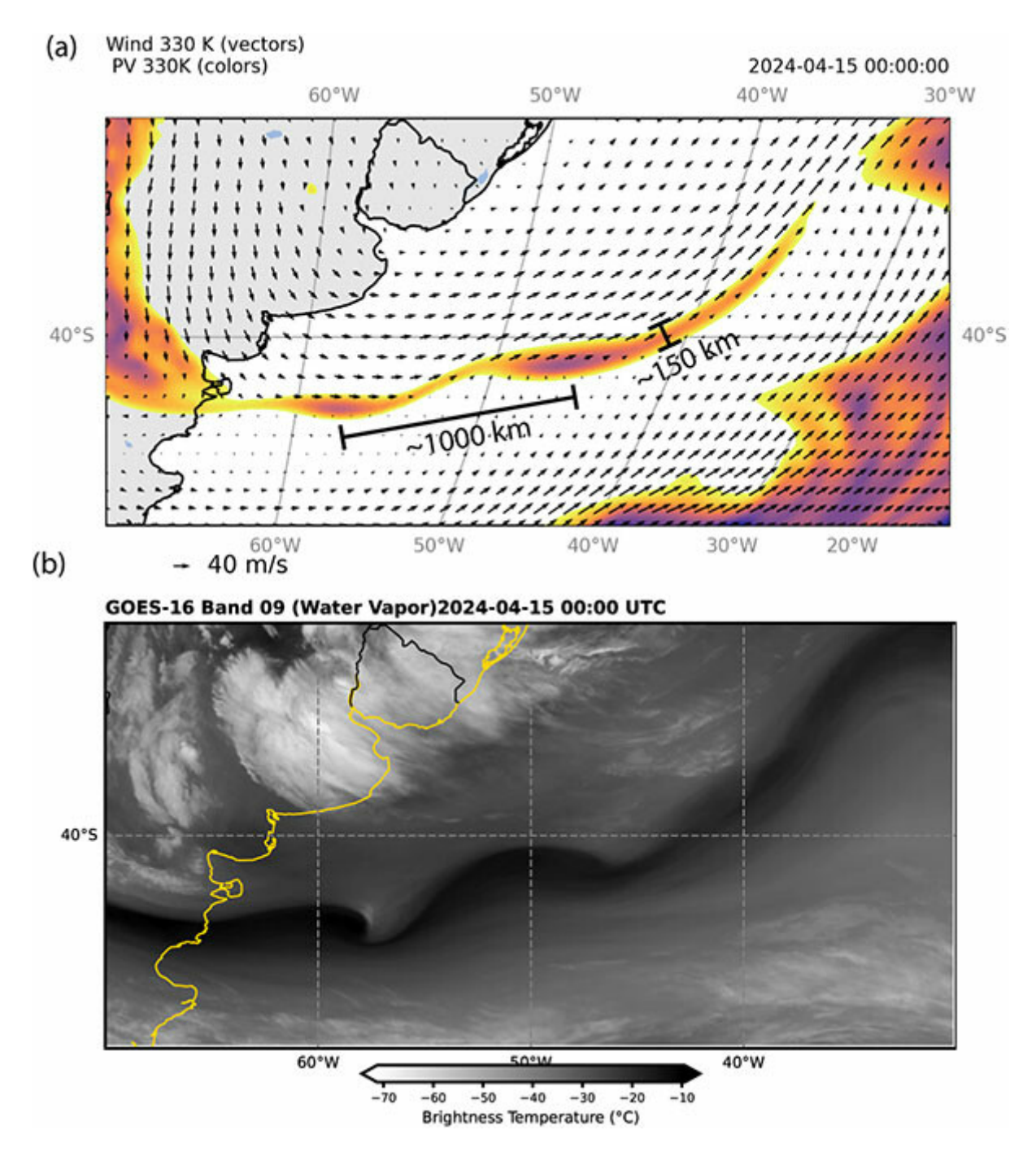


Figure 3. (a) A close-up view of the filament in Figure 2h from ERA5 re-analysis. (b) The corresponding mid-level water vapor channel (6.9 μm) image of the filament during April 15, 00 UTC, from GOES-16.

The advantages of this PV view should be evident. Just from looking at one single field, the formation of the cutoff low and its evolution as it segregates from the polar PV reservoir can be seen in a way completely analogous to ink in a tank experiment of fluid dynamics. However, many aspects of the evolution of the cutoff low need further exploration. First, because a single isentropic level, which is usually in the lower stratosphere, is being looked at, no major information on the coupling with the surface circulation is available from this field. If the cutoff low is considered as an upper level cyclonic PV perturbation (e.g., Holton, 2004), the vertical extent of the perturbation can be theoretically quantified using the Rossby scale height $H = \frac{fL}{N}$, where f is the Coriolis parameter,

L is the horizontal scale of the perturbation, and N is the Brunt-Väisälä frequency, a measure of static stratification. A peculiarity of the southeastern Pacific is that it is the coldest ocean at subtropical latitudes, which means it has a higher value of N compared to other regions of the planet at about the same latitude. This would result in lower values for H, and therefore, the upper level perturbations are relatively uncoupled from the surface west of the Andes. However, the decoupling of the upper level perturbation is in some sense nonlinear, given that the existence of stability precludes the development of surface and mid-level circulations and, therefore, might act to "protect" the upper level cyclone from their demise through diabatic heating (Garreaud & Fuenzalida, 2007). As the cutoff low approaches the Andes, the possibility of the release of potential instability through ascent becomes more likely, and therefore, diabatic heating over the Andes due to the precipitation produced by orographic lifting might contribute to the lysis of the cyclone. Presumably, turbulent mixing produced by the interaction between the perturbation and the topography also plays a role in destroying the cutoff low. Some of these features are explored in the following sections.

Vertical Structure

If a cross section of the low during April 13, 2024, 00 UTC, along 80°S (Figure 4), is considered, it can be seen that the PV anomaly can penetrate to the mid-levels of the atmosphere. High values of static stability are evident in the cyclonic PV region, where the isentropes are closely packed in the vertical. In contrast, the region immediately below the PV anomaly is a region of low static stability, consistent with the fact that the cutoff low corresponds to an upper level cold core. This implies that cold air in the mid- to upper levels of the atmosphere replaces otherwise warmer subtropical air, which tends to increase the static stability of the lower stratosphere and decrease the static stability of the lower troposphere. For example, during a case study in 2012, Rahn (2014) reported an increase in the height of the marine boundary layer from about 2 km to 4 km (and a complete disappearance of the subsidence temperature inversion) during the passage of a cutoff low. However, a decrease in static stability is usually not enough to produce deep convection over the ocean on the cold Pacific coast of southeastern South America. Even if convective towers develop, the small values of shear below the center of the upper-level low, prevent mesoscale organization (Rahn, 2014). In this particular case, the cyclonic circulation is seen to be confined to levels above 700 hPa, where the horizontal winds are higher than 10 m/s (Figure 4b). On the equatorward side of the cyclone, an upper level front is evident (marked as a blue line in Figure 4b). Along the front low values of specific humidity and cyclonic PV indicate a tropopause folding that occurs associated with the secondary circulation associated with the cutoff low (see, e.g., Pinheiro et al., 2020; Rondanelli, Gallardo, et al., 2002).

To understand the stability of the cutoff low, look at a single vertical profile at 30° S and 80° W on April 13, 2024, 00 UTC, in a SkewT-logp diagram (Figure 5a). It shows that a parcel on the surface is slightly unstable and exhibits some positive convective available potential energy (CAPE) values (~20 J/kg/K). However, these positive CAPE values are capped by a strong convective inhibition of magnitude similar to that of the CAPE. The lower positive CAPE values are confined to a shallow

layer between 900 and 850 hPa. A nearly isothermal layer between 800 and 750 hPa suggests the usual effect of subsidence warming over this region of the Pacific. Above the isothermal region, the temperature profile is absolutely stable.

Considering the sounding as a whole, surface parcels might develop much larger levels of CAPE through an increase in temperature or humidity, which could be relevant for the fate of the cutoff low on the eastward side of the Andes. Here, a vertical profile in the equatorial region of the low has been considered. This air column will be carried by the circulation and probably forced to ascend orographically over the steep coast of northern Chile. In this case, examining the stability of a layer, rather than a single parcel, is more appropriate (Iribarne & Godson, 1981).

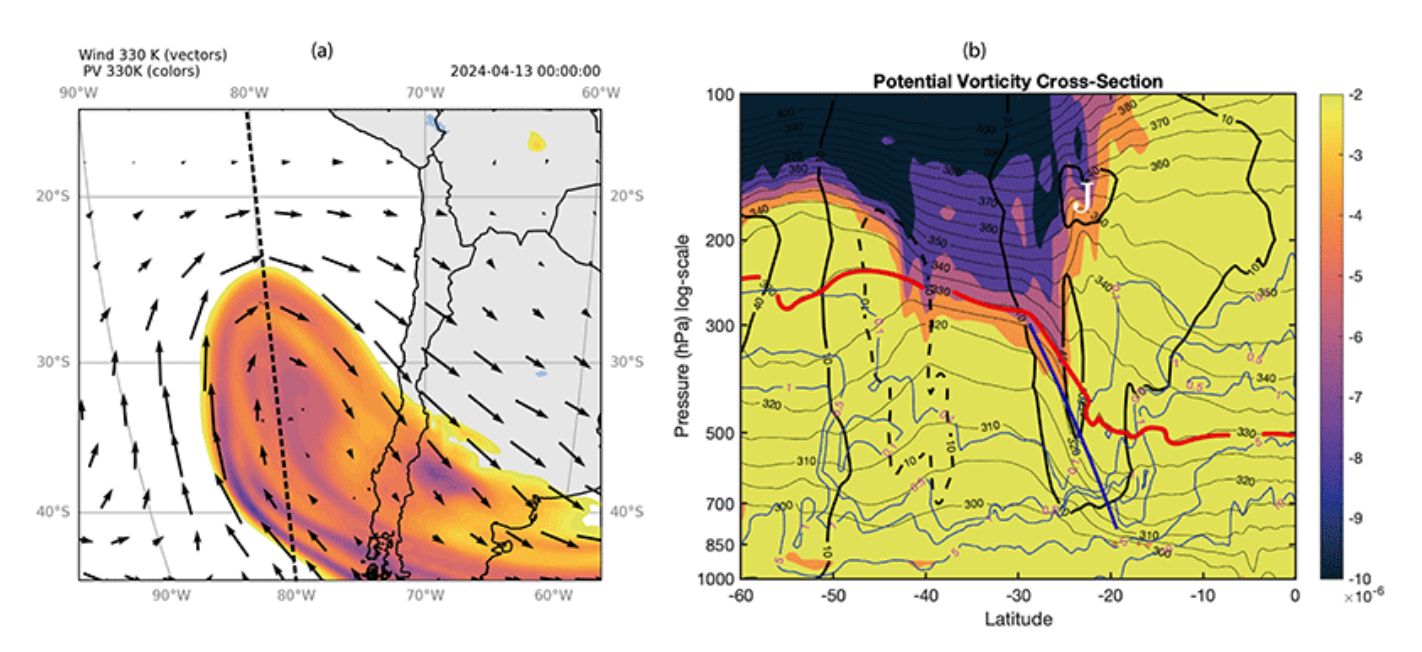


Figure 4. Cross section along 80°W of potential vorticity (colors) during April 13, 2024, 00 UTC. The black contours show the wind speed in the eastward (solid) and westward directions (dashed). Specific humidity (g kg⁻¹) is show in blue contours. Potential temperature is shown in thin black contours (K). The thick red line shows the 330-K isentrope. The blue slanted line indicates the approximate location of the upper level front, and the J marks the position of jet stream.

In Figure 5b, an initial layer of a depth of 150 hPa between points A (900 hPa) and B (750 hPa), which includes the stable inversion layer, is seen to have a lapse rate lower than moist adiabatic and is therefore absolutely stable. When considering the ascent of this finite layer by 200 hPa (which is roughly the height of the topography near the coast in northern Chile), the lower part of the layer becomes saturated, reaching point A' at 700 hPa. The B point never reaches saturation, so the ascent occurs along a dry adiabat. As a result, the ascent of the layer results in a lapse rate which is between a dry adiabat and a moist adiabat, leading to the conclusion that the profile is potentially unstable in this ascent. The potential instability of the profile has great explanatory power. If the profile were unstable over the ocean, deep convection would be released there, and the demise of the cutoff low would occur rapidly due to latent heating release and convective overturning. However, if the profile were absolutely stable, no convection would be expected to occur on the windward side of the Andes

as a result of topographical ascent. The potential instability is therefore "just right" to explain the behavior of most precipitating cutoff lows as they approach the Andes. However, Muñoz et al. (2020) studied the potential instability of the profiles, and they emphasize the role of the quasi-geostrophic ascent of the upper level cyclone as a major contributor to the release of potential instability, rather than the effect of the mostly blocked orographic ascent. Given the distribution of precipitation in individual cases and in the climatology (as seen in the following sections), the view that even moderate orographic ascent contributes to the release of the potential instability, probably acting in combination with the synoptic-scale forcing, tends to be favored. This is mainly due to the fact that precipitation from the cutoff low rarely peaks over the ocean, and therefore, the potential instability is released when the system faces the Andes. However, more research is needed to understand the precise mechanism of release of the potential instability.

Another interesting aspect is the ability of upper level perturbations to induce a surface cyclone. This is an important consideration, as the vertical extent of the upper level cyclone affects near-surface weather impacts and influences the system's ability to transport water vapor. For example, in the 2015 Atacama storm, a distinct near-surface cyclone was observed, confirmed by scatterometer data (Bozkurt et al., 2016). In contrast, this case study only reaches about 700 hPa, with substantial horizontal circulation (see Figure 4b). Nieto et al. (2005) found that approximately 50% of cutoff lows produce a surface cyclone, with even lower numbers reported for South America by Reboita and Veiga (2017). Furthermore, Barahona (2016) examined this issue, finding that approximately 55% of cutoff lows reach the 850-hPa level, and only 20% produce a closed cyclonic circulation at the surface.

The spatial distribution of the depth of the cutoff lows presented by Barahona (2016) appears to be consistent with the concept that the stability of the mean flow controls the depth of cutoff lows to some extent: Mid-latitudes exhibit deeper cutoff lows than the subtropics (as also shown by Barnes et al., 2021; Pinheiro et al., 2024). Moreover, deeper systems are more common in eastern than in western South America, although Pinheiro et al. (2024) observed the opposite pattern. Notably, because $H = \frac{fL}{N}$ may govern the depth of systems from the originating perturbation level, higher stability in the subtropics and western South America would generally lead to shallower systems.

Barnes et al. (2021) also identify fall as the season with deeper systems, aligning with lower environmental stability likely due to relatively warmer sea surface temperatures and cooler midtropospheric temperatures. Besides stability, the dynamical tropopause's location is significant, as perturbations originate at higher levels during summer, when the dynamical tropopause reaches greater geometric heights (Barnes et al., 2021). Finally, the baroclinicity of the mean flow may also affect the depth of the system, as upper level perturbations can amplify and interact with surface disturbances via baroclinic instability (Pinheiro et al., 2024).

Clouds and Precipitation Distribution

As discussed earlier, most of the precipitation activity of a cutoff low is expected to occur over the continent. Consistent with the release of potential instability, precipitation develops on the continent in part due to orographic ascent and predominantly over the poleward leading quadrant

of the low (Barahona, 2016; Pinheiro et al., 2020). From a quasi-geostropic perspective the equatorial side of the low can be seen as a jet streak with cyclonic curvature (see the geopotential at 300 hPa in Figure 6a). In such cases, the ascent is concentrated over the polar exit side of the jet streak (see, e.g., Muñoz & Schultz, 2021). This coincides with the large area of clouds observed to the southeast of the center of the low. Also interesting is that deep convective clouds show cloud top temperatures near -40°C on the windward side of the Andes (~300 hPa) but only appear on the continent. This was also the case, for example, during the strong cutoff low of March 2015, when satellite radar passages showed precipitation starting only within a few kilometers from the coast (Bozkurt et al., 2016).

Figure 6a shows that deep clouds are accompanied by lightning (marked with red crosses in the figure). There are isolated deep convective clouds near the center of the low; however, the main convective activity occurs over the diffluence region already identified. Deep convection directly associated with the cutoff low is concentrated on the windward side of the Andes. A passage of the Global Precipitation Measurement (GPM) satellite around April 13, 10 UTC, confirms that lightning occurs associated with precipitation bands, with instantaneous rainfall values close to 10 mm/h (Figure 7).

Spatial Distribution and Seasonality

Many algorithms have been developed over the years to identify cutoff lows in re-analysis data to construct climatologies and study the seasonality, spatial distribution, duration, and location of the genesis and lysis of these systems (e.g., Barahona, 2016; Favre et al., 2012; Fuenzalida et al., 2005; Ndarana & Waugh, 2010; Pinheiro et al., 2017, 2019; Reboita et al., 2010). The first important thing to mention is that in all these climatologies, southwestern South America is a region where a large frequency of cutoff lows occurs year-round, at about 30°S. In some of these climatologies (e.g., Favre et al., 2012), this region represents the maximum cutoff low frequency in the southern hemisphere.

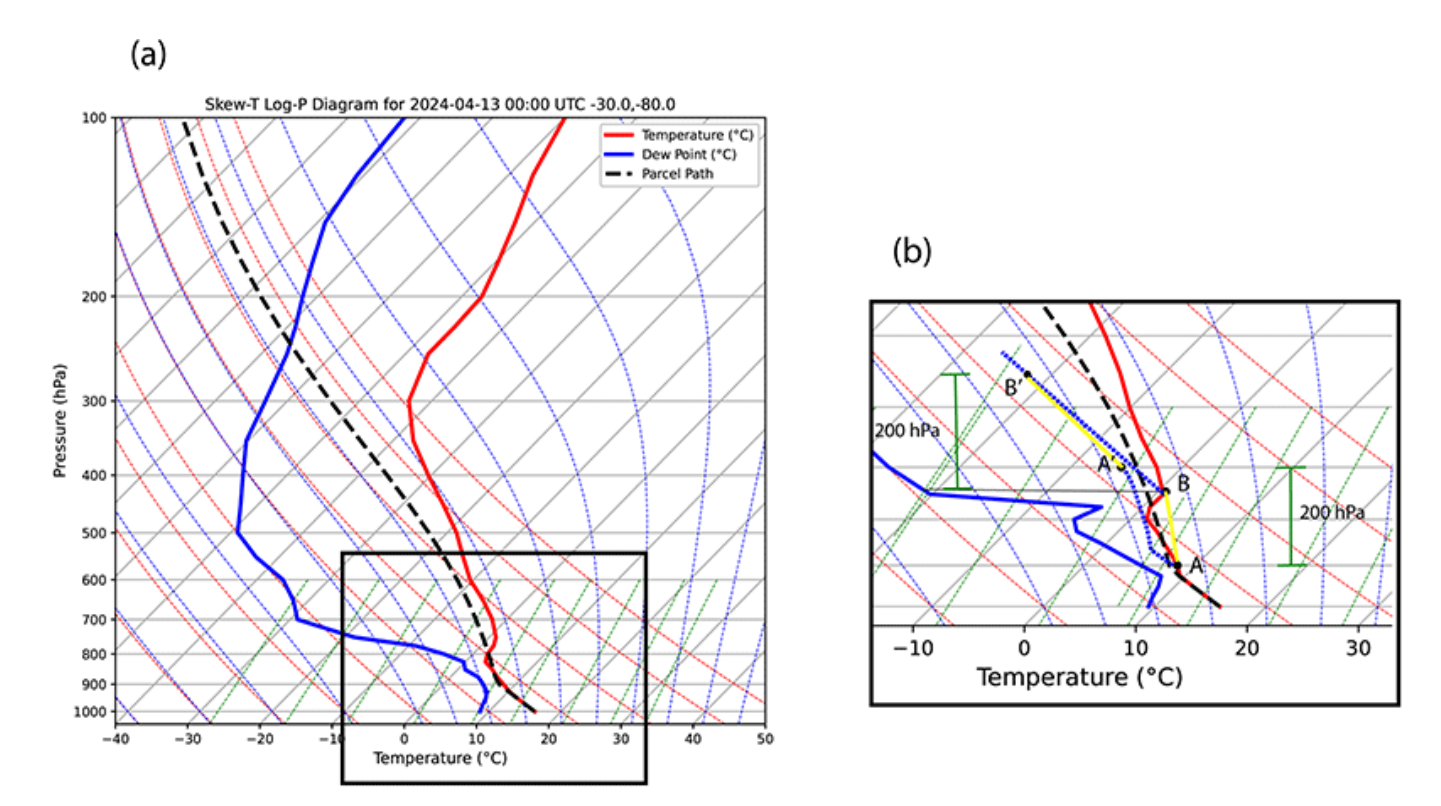


Figure 5. (a) SkewT-log p thermodynamic diagram of from an ERA5 re-analysis vertical profile from 30°S to 78°W during April 13, 2024, 00 UTC. The red thick line is the temperature, the blue thick line is the dewpoint temperature, and the dotted black line is the trajectory of a parcel from the surface. Red dotted lines are dry adiabats, blue dotted lines are moist adiabats, and green dotted lines are lines of constant saturation mixing ratio. Gray thick lines are isotherms. (b) Close-up of the region marked with a solid black rectangle in panel (a). The yellow lines show the mean lapse rate of the layers A–B and A′–B′. The thick dotted blue lines are the trajectories of parcels A and B when they ascend 200 hPa.

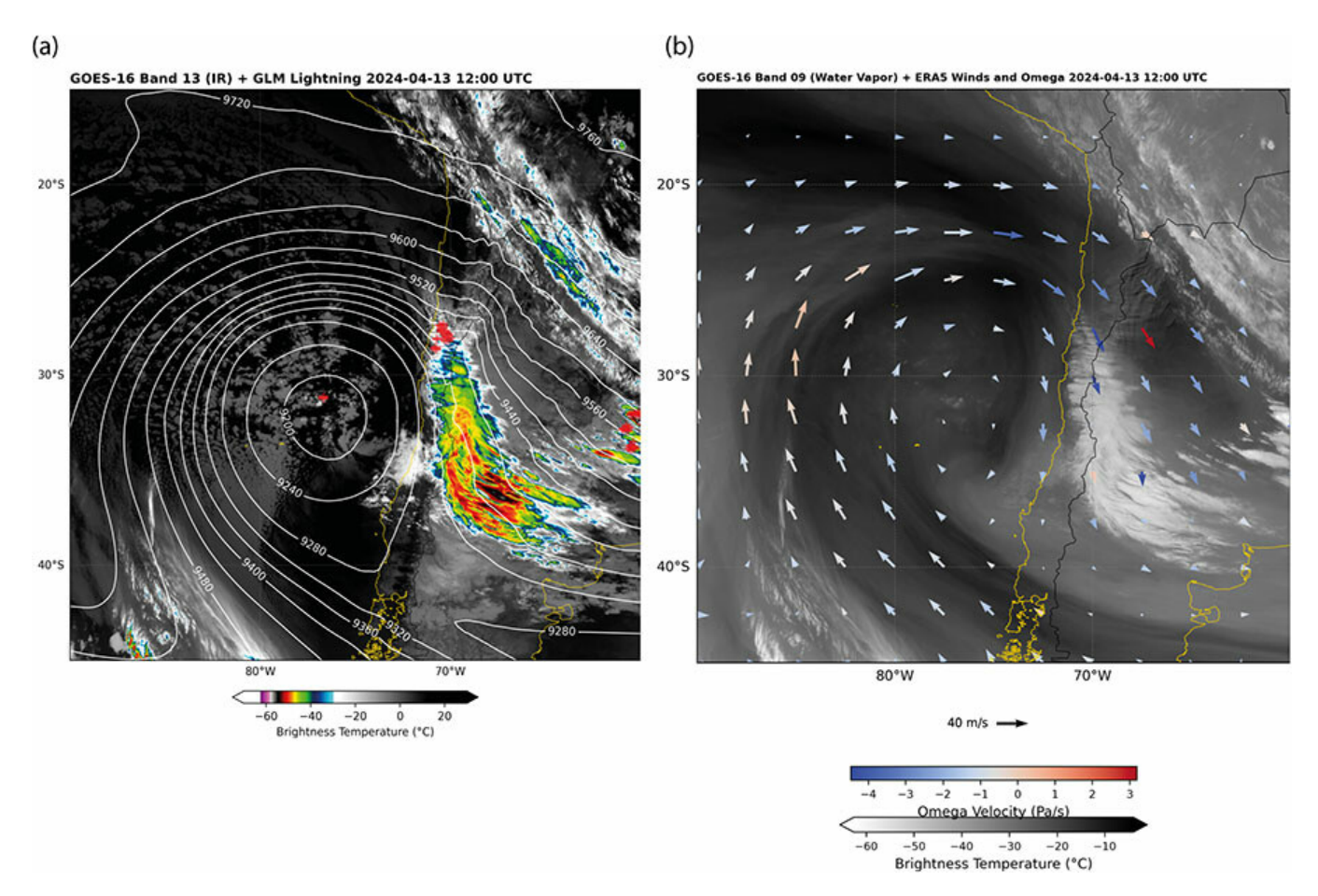


Figure 6. (a) Infrared window channel brightness temperature during April 13, 2024, 12 UTC. Lightning strikes are marked as red crosses from GOES Lightning Mapper. Geopotential height at 300 hPa is shown as white contours. (b) Water vapor channel image (brightness temperature in grayscale).

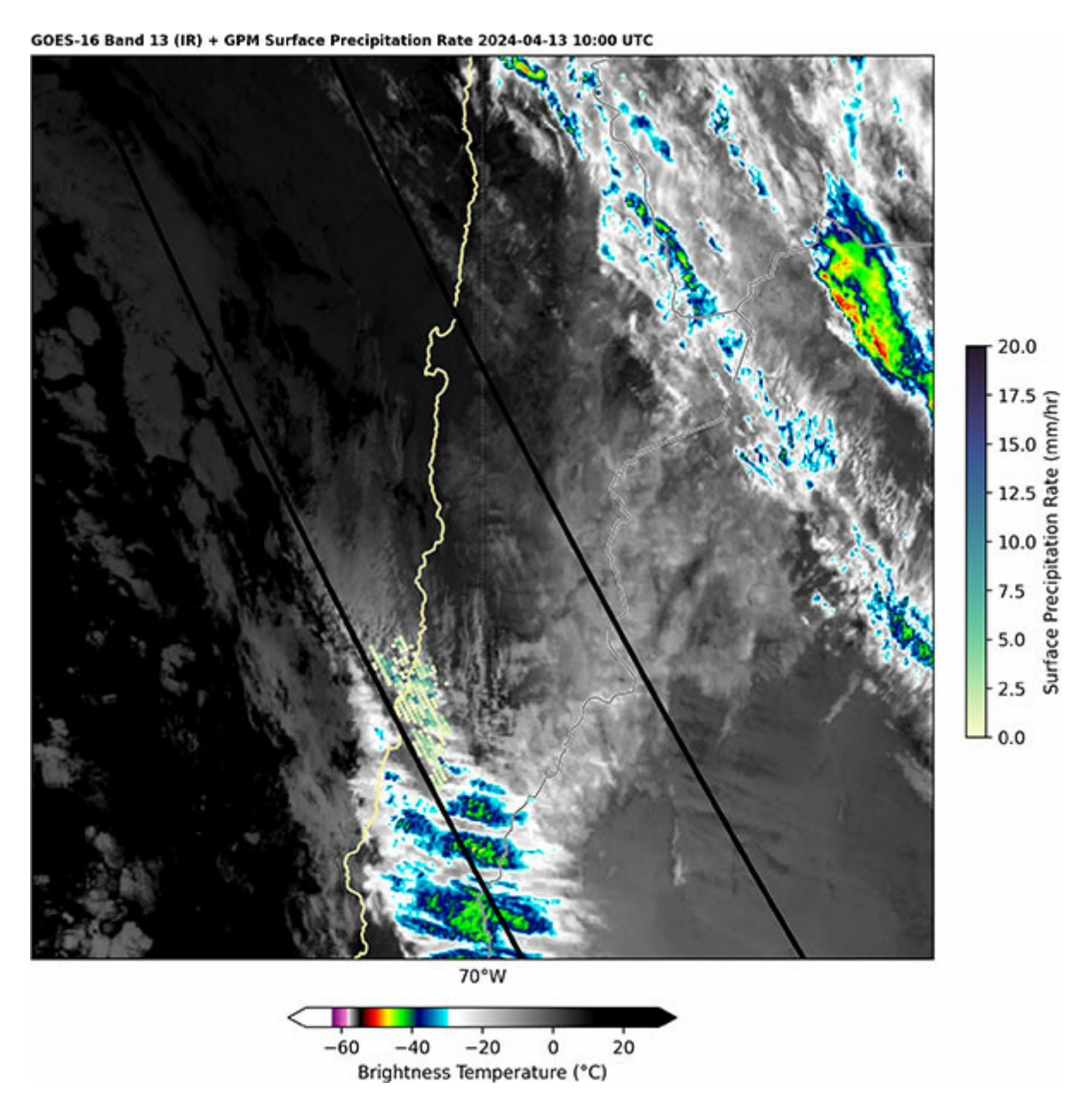


Figure 7. Infrared window channel brightness temperature during April 13, 2024, 10 UTC, from GOES-16. On top of the infrared images are radar-based surface precipitation estimates from the GPM satellite. Black lines show the width of the swath of the radar instrument.

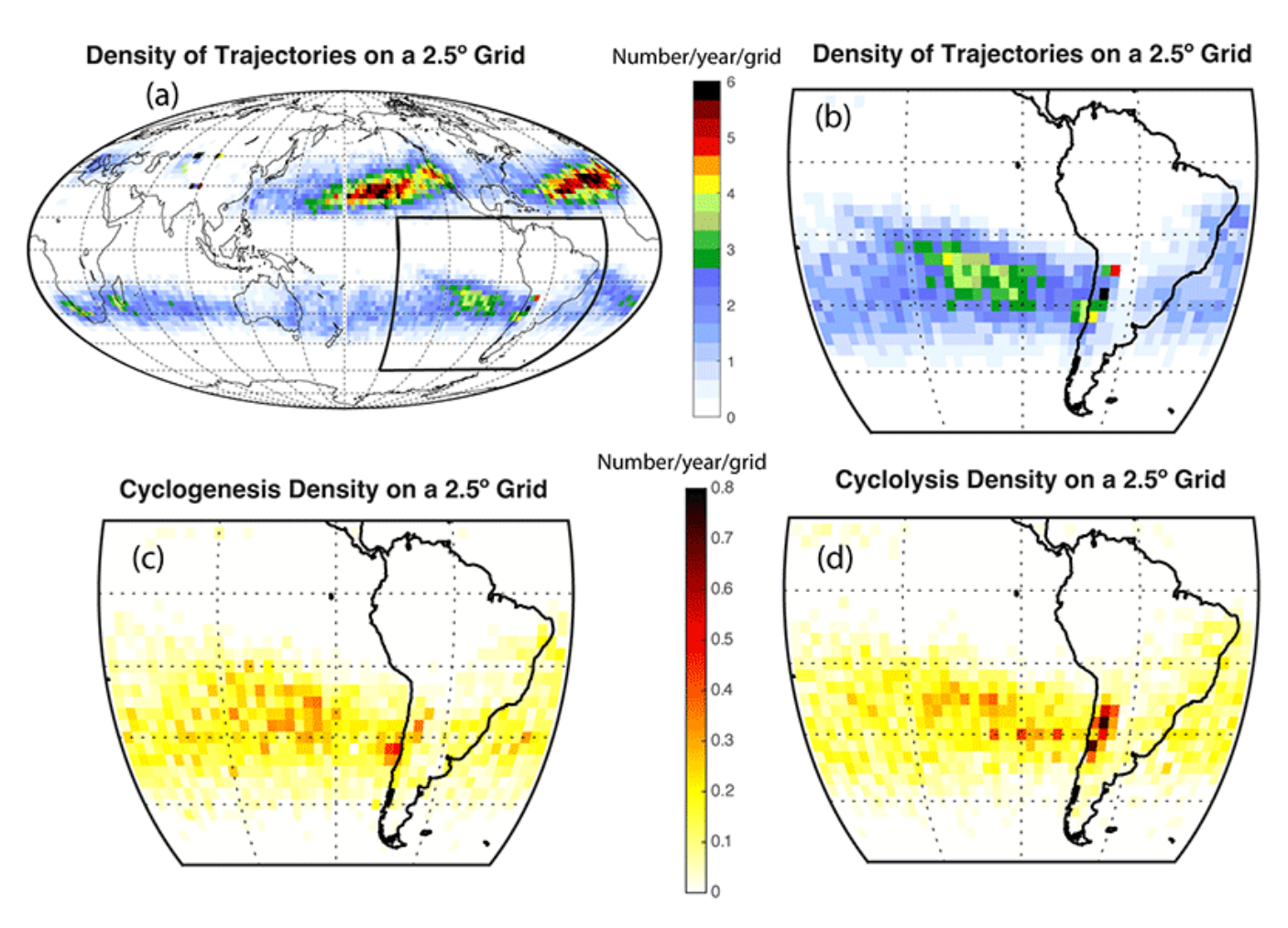


Figure 8. (a) Global climatology of the cutoff low frequency based on a climatology of cutoff lows using 300-hPa geopotential following criteria by Barahona (2016). The climatology was constructed using ERA5 re-analysis from 1979 to 2023. (b) Monthly seasonality of cutoff lows over South America (140°W to 30°W, based on the same climatology. (c) Annual frequency (number/year/grid) of points at the beginning of a cutoff low trajectory (cyclogenesis) and (d) at the end of the cutoff low trajectory (cyclolysis).

Following the work by Barahona (2016), a climatology covering the period 1979 to 2023 was constructed using the ERA5 re-analysis (Hersbach et al., 2020). The criteria for defining a cutoff low are as follows: The first criterion is the presence of a relative minimum in the gradient of the geopotential height at 300 hPa. The gradient between the minimum and a square region of $4^{\circ} \times 4^{\circ}$ must be larger than 40 gpm. The second criterion is that the thickness between 300 hPa and 600 hPa must also exhibit a relative minimum, ensuring the existence of a cold core. The minimum in this case must have a similar gradient between the center and the $4^{\circ} \times 4^{\circ}$ perimeter region, with a thickness difference of at least 15 gpm. The third criterion is that the identified cold core must be equatorward of the mean position of the jet stream during a particular month, indicating that the low is segregated from the mid-latitude westerlies. Finally, a criterion on the duration of the cutoff low is also applied: The minimum duration of the cutoff low must be 24 hours. Cutoff-low trajectories are then constructed by considering that the same cutoff low is being dealt with if,

during the next 6 hours, the cutoff low is within 10° of its previous position. Also filtered out are the cutoff lows that remain stationary within 1° during their life cycle to avoid including perturbations exclusively related to topography (e.g., Wernli & Sprenger, 2007).

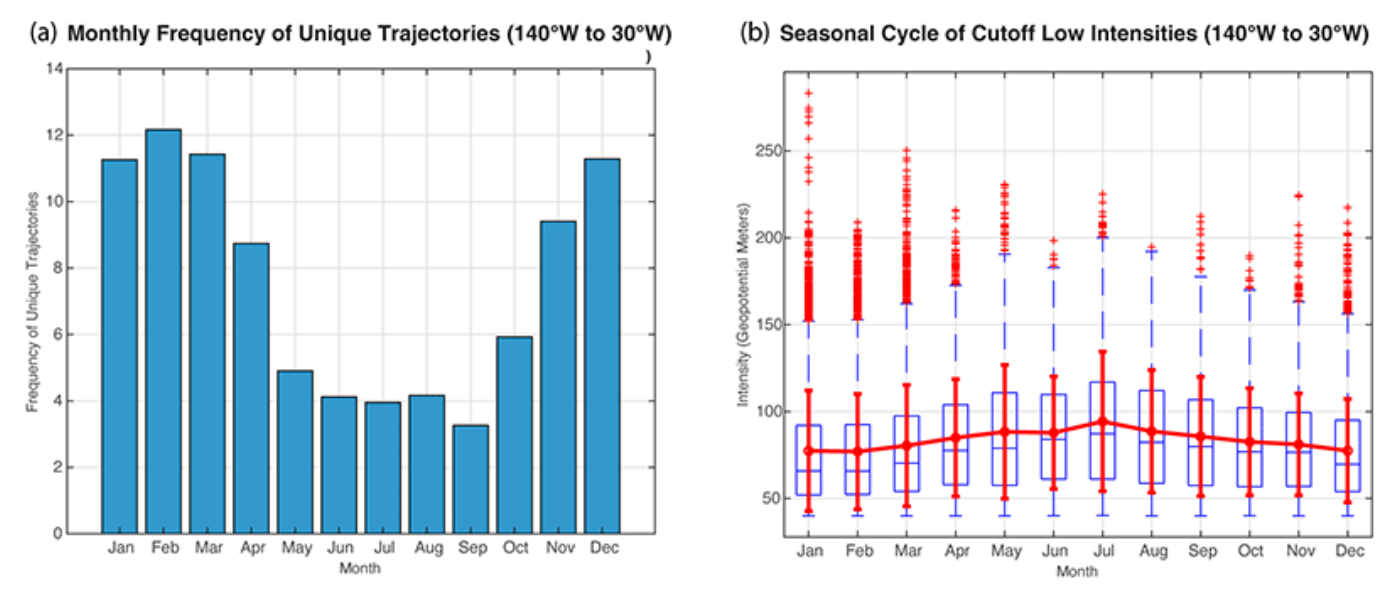


Figure 9. (a) Histogram of the annual frequency of cutoff lows for each month based on the ERA5 climatology of cutoff lows at 300 hPa from 1979 to 2023. (b) Box plot of the distribution of cutoff low intensities, measured as the difference in 300-hpa geopotential height of the center and the geopentential height of the perimeter of a concentric 4° latitude–longitude square.

As seen in Figure 8a, at 300 hPa, the cutoff-low area in southwestern South America shows prominent maxima with regions of about four cutoff lows per year or even more over the Andes. Looking closer Figure 8a, the region is composed of a maximum near the coast at around 30°S (e.g., Barnes et al., 2021; Favre et al., 2012; Fuenzalida et al., 2005) and a projection of this maximum toward the subtropical Pacific with a maximum at around 20°S, 100°W (Barnes et al., 2021; Portmann et al., 2021). It is interesting to note that early on these two "modes" in which cutoff lows can form in the southeastern Pacific, namely, the coastal cyclone and the south Pacific equatorward band, were recognized to have an impact in episodic spikes of ozone registered at mountain stations at 30°S (cases W and D, respectively, in Rondanelli, Gallardo, et al., 2002).

Another interesting aspect concerns cyclogenesis and cyclolysis. Figures 8c-d illustrate the density of the start and endpoint of each identified cutoff trajectory, which are referred to as cyclogenesis and cyclolysis, respectively. Both maps exhibit minimal differences, closely resembling the overall distribution of cutoff lows. This suggests that all areas are potential regions where a cutoff low can form or dissipate. However, the coastal region near 30°S appears to be a preferred region for cyclogenesis, whereas the leeward side of the Andes at 30°S is a preferred region for cyclolysis, as noted by several authors (Fuenzalida et al., 2005; Pinheiro et al., 2017, 2022). Cyclolysis in the lee of the Andes has several possible explanations. The first is the increase in friction experienced by the system while crossing the Andes, especially north of 30°S, where the average height of the Andes exceeds 5,000 m. A second possibility is the release of latent heat produced by precipitation as the

low crosses the Andes. On the lee side, the upper level perturbation induces southerly flow at the leading edge, rapidly transporting water vapor from tropical South America. This transport of water vapor induces precipitation and latent heat release, leading to upper level divergence, which weakens the cyclonic perturbation at upper levels (e.g., Garreaud & Fuenzalida, 2007; Pinheiro et al., 2022). Finally, the interaction between the cutoff low and a stationary ridge induced by topography has also been proposed as a weakening mechanism for the low (Funatsu et al., 2004). Regarding the genesis mechanisms, Pinheiro et al. (2022) identify the coastal region as an area of significant convergence of ageostrophic flux during the stage of formation of the cutoff lows. One might consider the role of topography in this flux convergence, as the dominant westerly flow impinging on the Andes is blocked and diverted southward (Kalthoff, Bischoff–Gauß, et al., 2002), generating cyclonic relative vorticity and ageostrophic convergence poleward of the subtropical jet stream.

Table 1. Summary of Studies on Cutoff Lows (COLs) Characteristics

Work	Variable/Level	Domain	Re-analysis	Period	Мах	Min	Number of COLs per year
Fuenzalida et al. (2005)	Z 500 hPa	SA 140°W-0	NCEP-NCAR	1969–1999	Autumn	Summer	10-20
Campetella and Possia (2007)	Z 250 hPa	SA 100°W-20°W	NCEP-NCAR	1979–1988	Autumn	Summer	10-25
Reboita et al. (2010)	Z 200 hPa	SA 130°W-20°W	NCEP-NCAR	1979–1999	Autumn	Winter	22.1
	Z 300 hPa	SH	NCEP-NCAR	1979–1999	Autumn	Summer	54.4
Ndarana and Waugh (2010)	Z 250 hPa	SH Subtropics	NCEP-NCAR	1979–2008	Summer	Winter	~50
Favre et al. (2012)	Z 500 hPa	SH	NCEP-NCAR	1979–2008	Autumn	Winter	330
Pinheiro et al. (2017)	ζ 300 hPa	SA 140°W-20°W	ERA-Interim	1979-2014	Autumn	Winter	50-90
Barahona (2016)	Z 300 hPa	SH	NCEP-NCAR	1998-2014	Autumn	Winter	142
Muñoz et al. (2020)	Z 200 hPa	SA 120°W-30°W	NCEP-NCAR	1979–2017	Summer	Winter	13
	Z 500 hPa	SA 120°W-30°W	NCEP-NCAR	1979–2017	Winter	Summer	25
This study	Z 300 hPa	SH 140°W-30°W	ERA-5	1979-2023	Summer	Winter	90

Note: Z is the geopotential height, ζ is the relative vorticity, SA is South America, and SH is the southern hemisphere.

From Table 1, it can be seen that there is a wide range of approaches for defining the climatology of cutoff lows. Therefore, some of the features of the climatologies are expected to be dependent on the particular definition of the systems, as well as the horizontal resolution of the re-analysis data and the main level of the atmosphere where perturbations are defined (Muñoz et al., 2020; Pinheiro et al., 2017; Reboita et al., 2010). However, some common characteristics arise, for example, where upper tropospheric levels are chosen, the seasonal maxima are found in summer and early autumn, while the minimum frequency of cutoff lows is found during winter (Barahona, 2016; Ndarana & Waugh, 2010; Pinheiro et al., 2017; Reboita et al., 2010). An almost opposite seasonality is found when the 500-hPa level is considered, where maxima occur during autumn and winter and minima during summer (Fuenzalida et al., 2005; Muñoz et al., 2020). In the constructed climatology, only a third of the number of cutoff lows during the winter minimum is detected compared to the frequency found during the summer maximum (Figure 9), consistent with previous work using a similar pressure level (Table 1). This level-dependent seasonality in the frequency of cutoff could be in part due to an artifact of selecting a single level for the analysis of the perturbations. In fact, Portmann et al. (2021) use a level-independent climatology in which they identify "PV cutoffs" at any isentropic level between 275 and 360 K. In their analysis, the South Pacific equatorward band shows a maximum frequency of cutoff lows of about 10% during summer and 3% during winter, whereas the coastal region shows a summer maximum as well of approximately 9% compared to the minimum 6% in winter. The summer minimum therefore found in climatologies using 500 hPa can be explained simply by the fact that during the summer the level of formation of the cutoff lows reaches higher levels (Barnes et al., 2021; Portmann et al., 2021; Wernli & Sprenger, 2007). This is also a warning for studies that attempt to look at trends in the frequency of these systems in the future and the past, where changes in the level of formation of cutoff lows might be misinterpreted as changes in the frequency of these systems.

The mean intensity of the cutoff lows also appears to have a seasonal cycle at 300 hPa, with a slight increase in the mean intensity of the systems during winter and a minimum during summer (Figure 8). Again, this behavior of the systems might be influenced by the single-level selection made in this case. During winter, the 300-hPa level is lower than during summer, possibly capturing more intense systems, although some outliers during summer display larger gradients. A complete understanding of the seasonality of cutoff lows is lacking at this time, as a complete three-dimensional analysis of the formation of these systems is needed (e.g., Lakkis et al., 2019; Portmann et al., 2021). Presumably, even if no seasonality of upper level formation was detected, seasonality of the tropospheric stability and the height of the perturbations will induce a different effect on the surface weather, a matter that needs further exploration.

Moisture Dynamics and Precipitation

During an early stage of the research on cutoff lows, at least until the work of Garreaud and Fuenzalida (2007), little was understood about the interaction of the cutoff low with the surrounding moisture field. In fact, emphasis on the dry dynamical features of these systems usually led to conflicting forecasts regarding the ability of the cutoff low to produce precipitation over the windward side of the Andes.

Fuentes (2014) compared two mesoscale simulations of a case study of a cutoff low in central Chile and—perhaps for the first time—identified the source of water vapor of the cutoff low as coming from a water vapor streamer originating in the coast of Peru and northern Chile during March 2008. In particular, he used two different re-analysis data sets as boundary conditions for the simulation, one re-analysis representing a slightly dryer condition along this streamer and therefore producing less precipitation in the corresponding simulation. In March 2015, northern Chile experienced one of the major hydrometeorological disasters when a cutoff low was able to tap water from the rather warm coastal waters of Peru at the beginning of El Niño 2015–2016. It was then immediately clear that a similar mechanism as in the case study of Fuentes (2014) was at play in this case, namely, the transport of water vapor in a water vapor streamer trapped along the coast, being fed by the strong southerly circulation in the leading edge of a cutoff low (Barrett et al., 2016; Bozkurt et al., 2016). To borrow from chemistry, the limiting reagent for this extreme storm was not circulation but water vapor. For instance, the 500-hPa anomaly for the March 2015 storm was only one standard deviation below climatology (Barrett et al., 2016); therefore, many upper level storms with a similar circulation anomaly would be expected over a period of several years; however, the peak discharge of the storm estimated for several basins in northern Chile was the largest documented over a period of several decades and without any precedent (Wilcox et al., 2016). Also, the large sensitivity of the precipitation to the sea surface temperature over the Peruvian coast in the modeling study carried out by Bozkurt et al. (2016) is also suggestive of the little relative importance of the dry dynamical anomaly with respect to the water vapor anomaly, in setting the extreme precipitation experienced during this event.

With this knowledge in mind, Barahona (2016) classified cutoff lows in the southern hemisphere according to their precipitable water and gradient intensity based on the geopotential height of 300 hPa. From his composites, it is clear that even very strong circulation anomalies in 300 hPa (gradients of the order of 300 m/10°) combined with precipitable water in the lower 20th percentile of the distribution, produce precipitation confined to a small sector at the poleward (difluent) leading edge of the cutoff low. However, low circulation gradients of even less than 100 m over 10° for systems in the upper 80th percentile of precipitable water produce a large region of precipitation that extends over most of the leading edge area (as in Figure 6a in this case study). Similarly, Muñoz and Schultz (2021) studied cutoff lows in the southeast Pacific based on surface precipitation at 94 surface stations. They classified systems from 1979 to 2017 into LOW25 and HIGH25 depending on whether precipitation was in the lower or higher quartiles of the precipitation distribution for cutoff lows based on surface station data. They found that synoptic vertical forcing in both cases was not significantly different and therefore could not explain the difference in precipitation found between these systems. They attributed the difference between these systems to a better defined and stronger "moisture plume" feeding the cutoff lows in the HIGH25 quartile cases, in line with previous research indicating the critical role of water vapor availability in the resulting precipitation. Figure 10 shows a cross section along 26°S for three of the cases already mentioned. The first corresponds to the case studied by Fuentes (2014), the second is the Atacama storm of March 2015, and the third is the case study presented in this article. In all three cases, a noticeable presence of the coastally trapped moisture plume originating in front of the coast of Peru, extending even to southern Chile in the most extreme cases, can be seen. This coastally trapped moisture plume is characteristic of precipitating cutoff lows. Presumably, once the leading edge of the cutoff

low begins to approach the continent, the southerly circulation at the leading edge reinforces the southerly barrier jet that results from the blocking of the flow by the Andes, which is usually located between 2,000 and 4,000 m (Kalthoff, Bischoff–Gauß, et al., 2002). In all three cases, meridional winds can be seen to peak in the lower troposphere closer to the Andes barrier and, in Figures 10a and 10b, display a maximum of approximately 15 m/s at about 750 hPa and with relatively high humidity values up to at least the level of 600 hPa for the Atacama storm —which constitutes the most extreme member of this set. This relatively deep layer of water vapor is then effectively transported southward producing strong values of integrated vapor transport values (larger than 200 kg/m/s). Perhaps not coincidentally, all these cases occur at the end of summer and the beginning of fall, when sea surface waters along the coast of Peru reach their maximum annual temperature.

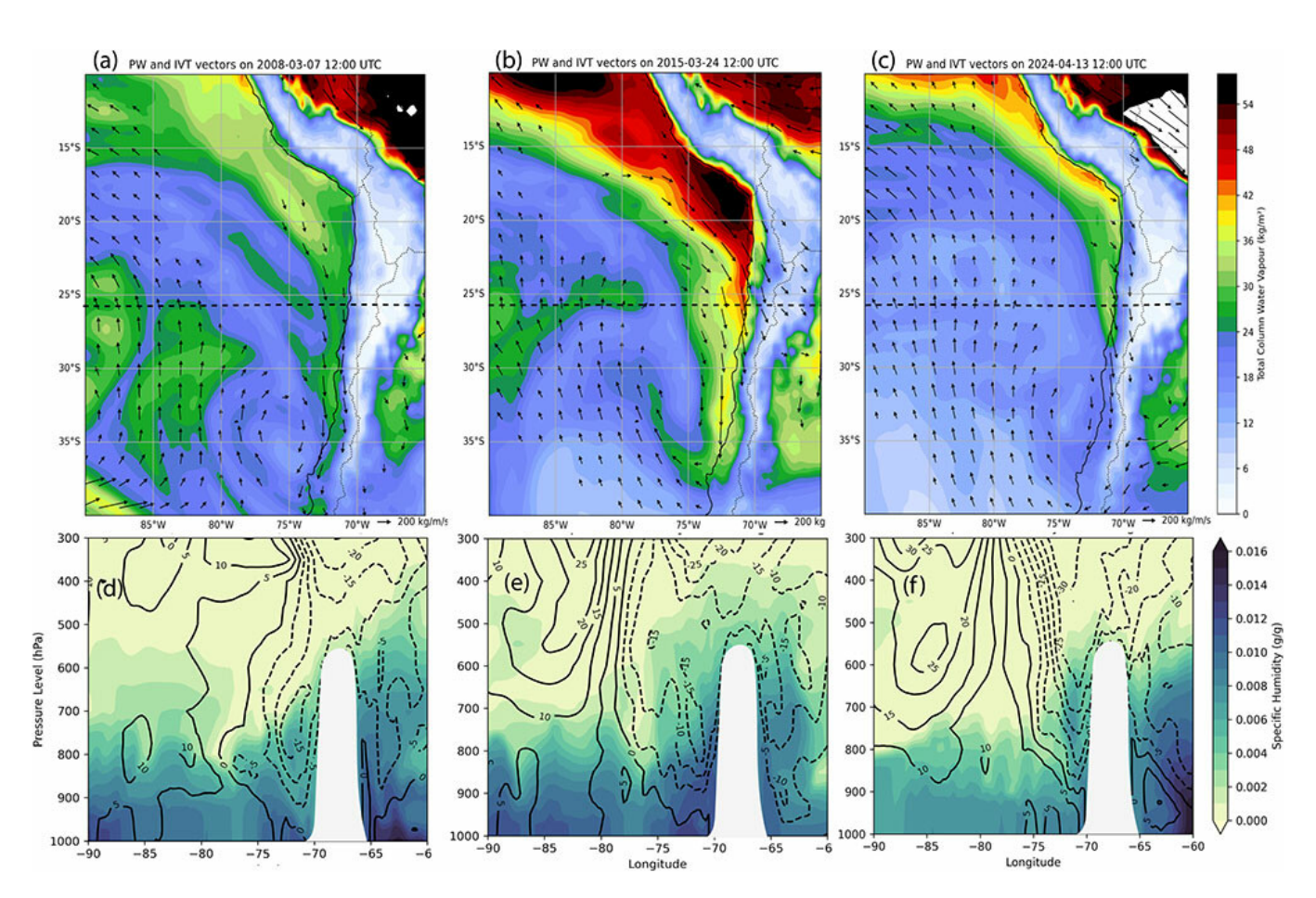


Figure 10. (a), (b), and (c) are maps of the precipitable water (colors) and integrated water vapor transport (vectors) for March 7, 2008; March 24, 2015; and April 13, 2024, respectively. (d), (e), and (f) are cross sections of specific humidity (colors) and meridional wind component (solid and dashed contours for positive and negative values, respectively) for the same dates as the upper panels.

Using the climatology of cutoff lows presented in the previous section, the distribution of rainfall due to cutoff lows and the fraction that this rainfall represents with respect to the total rainfall having been recalculated, as done by Aceituno et al. (2021). Despite the cutoff lows climatology closely following that of Barahona (2016), a larger number of cutoff lows were found in this study,

perhaps due to the use of a higher resolution re-analysis. It was found that annual precipitation peaks at about 300 mm on the leeward side of the Andes (Figure 11a). Many places along the Andes show precipitation larger than 100 mm from about 28°S to 38°S. The rainfall distribution due to cutoff lows has a very distinct orographic pattern with a minimum near the coast and a maximum over the leeward side of the southern Andes. Also notable is that most of the precipitation in the hyper-arid core of Atacama is explained by cutoff lows (see Figure 1a and Figure 11b). The maximum percentage peaks at about 25°S (Figure 11d) and is higher than 50% north of 30°S on the windward side. A large area of influence on the leeward side of the Andes can also be discerned, where most of the annual precipitation appears associated with cutoff lows, presumably due to the modulation of cutoff lows on the convective activity during summer.

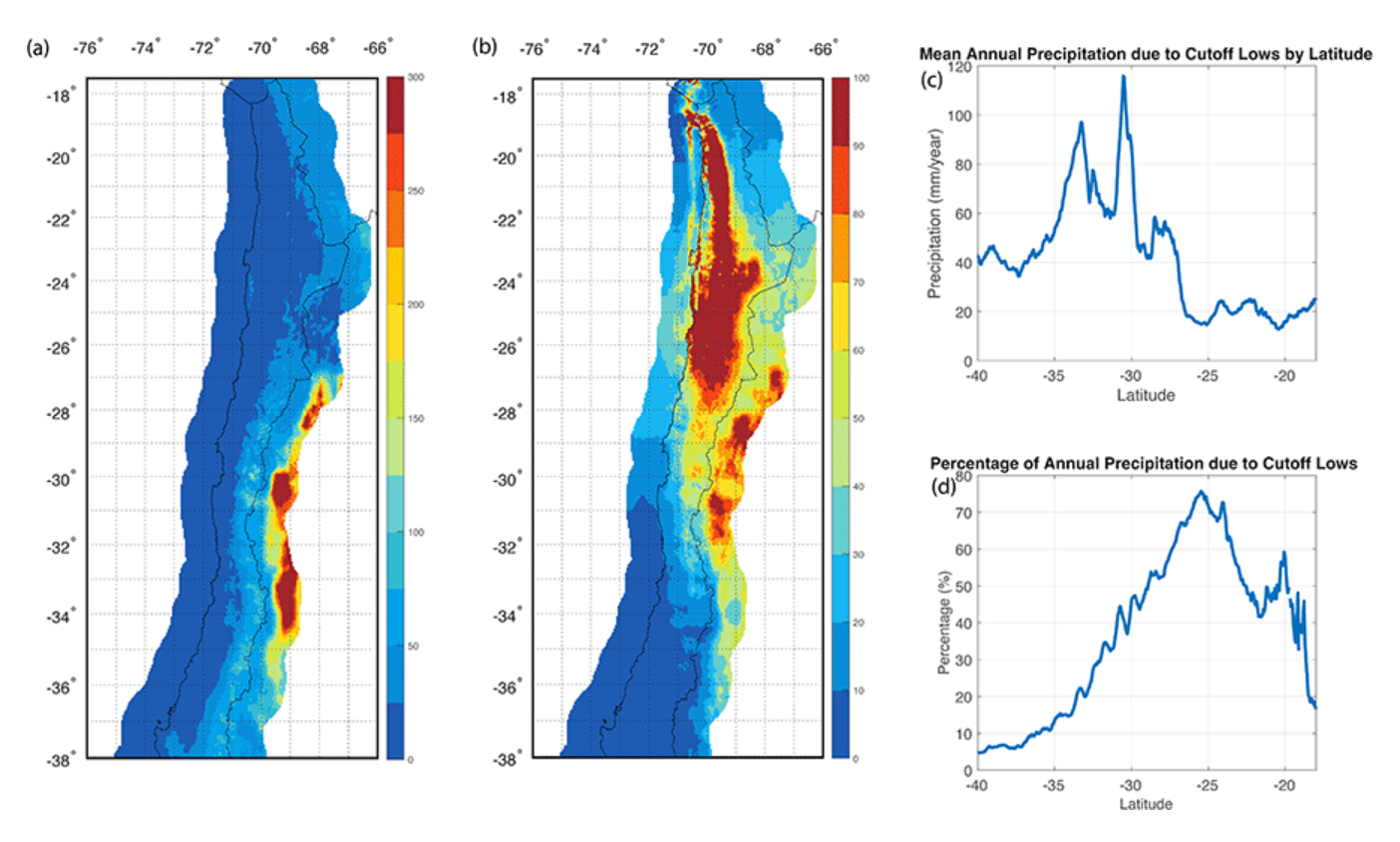


Figure 11. Rainfall distribution due to cut-off lows from CR2Met database from 1979 to 2021 (Boisier, 2023; Boisier et al., 2018) (a) Annual precipitation due to cutoff lows (mm). (b) Percentage of cutoff low rainfall respect to total rainfall. (c) Latitude distribution of the mean annual precipitation due to cutoff lows. (d) Latitude distribution of the percentage rainfall due to cutoff lows.

Outlook

Cutoff lows in southwestern South America are significant because they are the main drivers of extreme precipitation events in this region. They represent the main mechanism through which the extreme dryness and stability of the Atacama Desert can break down, potentially bringing rain to this otherwise hyper-arid desert. As discussed, cutoff lows are very frequent in this part of the world. The lack of precipitation due to these systems is often associated more with the relatively dry

climatological water vapor over this region than with the absence of synoptic-scale perturbations. For example, Lagos-Zúñiga et al. (2024) have shown an increase of approximately 1.5 mm per decade in precipitable water over the source region of Peru during the fall, which is consistent with an increasing trend for daily precipitation extremes north of 30°S during the same season. Climate change is expected to increase the availability of water vapor in the region, which is considered the main source of moisture for these systems.

Furthermore, Muñoz et al. (2020) documented an upward trend in the number of cutoff lows, attributing this to the poleward shift of the mid-latitude jet, which increases the likelihood of anticyclonic wave breaking (Rivière, 2011), the primary mechanism for the formation of cutoff lows. Given the very low precipitation in the arid regions of northern Chile, even a few extreme cases can significantly influence the climatology of precipitation over decades. Therefore, a more detailed understanding of the mechanisms behind these specific events can provide insight into the future behavior of these systems.

In particular, the future of arid northern Chile under climate change must be carefully considered. Modeling studies often do not focus on the specific processes that produce precipitation in various model projections. However, some studies indicate an increase in extreme rainfall in this region (e.g., Ortega et al., 2019). A crucial focus of research should be to better understand both the processes that produce these cutoff lows, such as the role of intense tropical perturbations in triggering Rossby wave-breaking events (e.g., Barnes et al., 2021; Rondanelli et al., 2019), and the mechanisms by which cutoff lows release potential instability and transport water vapor to generate extreme precipitation events. A detailed process-oriented understanding of global projections will provide more confidence in predicting the sign and magnitude of precipitation changes in areas where cutoff lows are the dominant synoptic-scale mechanism of precipitation.

References

Aceituno, P., Boisier, J. P., Garreaud, R., Rondanelli, R., et al. (2021). Climate and weather in Chile https://doi.org/10.1007/978-3-030-56901-3_2. In B. Fernández & J. Gironás (Eds.), Water resources of Chile (Vol. 8, pp. 7–27). World Water Resources.

Appenzeller, C., Davies, H. C., & Norton, W. A. (1996). Fragmentation of stratospheric intrusions. *Journal of Geophysical Research*, 101(D1), 1435–1456.

Barahona, C. E. (2016). *Precipitación asociada a bajas segregadas en el hemisferio sur* [Master's thesis, Universidad de Chile].

Barnes, M. A., Ndarana, T., & Landman, W. A. (2021). Cut-off lows in the southern hemisphere and their extension to the surface. *Climate Dynamics*, *56*(11–12), 3709–3732.

Barrett, B. S., Campos, D. A., Veloso, J. V., et al. (2016). Extreme temperature and precipitation events in March 2015 in central and northern Chile. *Journal of Geophysical Research D: Atmospheres*, *121*(9), 4563–4580.

Belmadani, A., Echevin, V., Codron, F., Takahashi, K., & Junquas, C. (2014). What dynamics drive future wind scenarios for coastal upwelling off Peru and Chile? *Climate Dynamics*, 43(7–8), 1893–1914.

Boisier, J. P. (2023). *CR2MET: A high-resolution precipitation and temperature dataset for the period 1960–2021 in continental Chile (v2. 5)* [Data set]. Zenodo.

Boisier, J. P., Alvarez-Garretón, C., Cepeda, J., Osses, A., Vásquez, N., & Rondanelli, R. (2018). CR2MET: A high-resolution precipitation and temperature dataset for hydroclimatic research in Chile. In *EGU general assembly conference abstracts* (p. 19739). European Geosciences Union.

Bozkurt, D., Rondanelli, R., Garreaud, R., & Arriagada, A. (2016). Impact of warmer eastern tropical pacific SST on the March 2015 Atacama floods. *Monthly Weather Review*, *144*(11), 4441–4460.

Campetella, C. M., & Possia, N. E. (2007). Upper-level cut-off lows in southern South America. *Meteorology and Atmospheric Physics*, 96(1), 181–191.

Favre, A., Hewitson, B., Tadross, M., Lennard, C., & Cerezo-Mota, R. (2012). Relationships between cut-off lows and the semiannual and southern oscillations. *Climate Dynamics*, *38*(7), 1473–1487.

Fuentes, R. (2014). Sensibilidad a diferentes condiciones iniciales en simulaciones de mesoscala de una baja segregada: Caso de estudio [Doctoral dissertation, Universidad de Valparaíso].

Fuenzalida, H. A., Sánchez, R., & Garreaud, R. D. (2005). A climatology of cutoff lows in the southern hemisphere. *Journal of Geophysical Research D: Atmospheres*, *110* (D18), D18101.

Funatsu, B. M., Gan, M. A., & Caetano, E. (2004). A case study of orographic cyclogenesis over South America. *Atmósfera*, *17*(2), 91–113.

Garreaud, R., & Fuenzalida, H. A. (2007). The influence of the Andes on cutoff lows: A modeling study. *Monthly Weather Review*, *135*(4), 1596–1613.

Godoy, A. A., Possia, N. E., Campetella, C. M., & García Skabar, Y. (2011). A cut-off low in southern South America: Dynamic and thermodynamic processes. *Revista Brasileira de Meteorologia <u><https://www.researchgate.net/journal/Revista-Brasileira-de-Meteorologia-0102-7786?</u>*

_tp=ey.Jjb250ZXh0ljp7ImZpcnN0UGFnZSI6InB1YmxpY2F0aW9uliwicGFnZSI6InB1YmxpY2F0aW9uln19>, 26(4), 503-514.

Hersbach, H., Bell, B., Berrisford, P., Hirahara, S., Horányi, A., Muñoz-Sabater, J., Nicolas, J., Peubey, C., Radu, R., Schepers, D., Simmons, A., Soci, C., Abdalla, S., Abellan, X., Balsamo, G., Bechtold, P., Biavati, G., Bidlot, J., Bonavita, M., . . . Thépaut, J.-n. (2020). The ERA5 global reanalysis. *Quarterly Journal of the Royal Meteorological Society*, 146(730), 1999–2049.

Holton, J. R. (2004). An introduction to dynamic meteorology. Elsevier.

Hoskins, B. J., McIntyre, M. E., & Robertson, A. W. (1985). On the use and significance of isentropic potential vorticity maps. *Quarterly Journal of the Royal Meteorological Society*, *111*(470), 877–946.

Iribarne, J. V., & Godson, W. L. (Eds.). (1981, December). Atmospheric thermodynamics. Kluwer Academic.

Kalthoff, N., Bischoff-Gauß, I., et al. (2002). Mesoscale wind regimes in Chile at 30 S. *Journal of Applied Meteorology and Climatology*, *41*, 953–970.

Lagos-Zúñiga, M., Mendoza, P. A., Campos, D., & Rondanelli, R. (2024). Trends in seasonal precipitation extremes and associated temperatures along continental Chile. *Climate Dynamics*, 62(5), 4205–4222.

Lakkis, S. G., Canziani, P., Yuchechen, A., Rocamora, L., Caferri, A., Hodges, K., & O'Neill, A. (2019). A 4D feature-tracking algorithm: A multidimensional view of cyclone systems. *Quarterly Journal of the Royal Meteorological Society*, 145(719), 395–417.

McIntyre, M. E. (2003). Potential vorticity. Encyclopedia of Atmospheric Sciences, 2, 685–694.

Muñoz, C., Schultz, D., & Vaughan, G. (2020). A midlatitude climatology and interannual variability of 200- and 500-hPa cut-off lows. *Journal of Climate*, 33(6), 2201–2222.

Muñoz, C., & Schultz, D. M. (2021). Cutoff lows, moisture plumes, and their influence on extreme-precipitation days in Central Chile. *Journal of Applied Meteorology and Climatology*, 60(4), 437–454.

Ndarana, T., & Waugh, D. W. (2010). The link between cut-off lows and Rossby wave breaking in the southern hemisphere. *Quarterly Journal of the Royal Meteorological Society*, 136(649), 869–885.

Nieto, R., Gimeno, L., de la Torre, L., Ribera, P., Gallego, D., García-Herrera, R., García, J. A., Nuñez, M., Redaño, A., & Lorente, J. (2005). Climatological features of cutoff low systems in the northern hemisphere. *Journal of Climate*, *18*(16), 3085–3103.

Oerder, V., Colas, F., Echevin, V., Codron, F., Tam, J., & Belmadani, A. (2015). Peru-Chile upwelling dynamics under climate change. *Journal of Geophysical Research: Oceans*, *120*(2), 1152–1172.

Ortega, C., Vargas, G., Rojas, M., Rutllant, J. A., Muñoz, P., Lange, C. B., Pantoja, S., Dezileau, L., & Ortlieb, L. (2019). Extreme ENSO-driven torrential rainfalls at the southern edge of the Atacama Desert during the late Holocene and their projection into the 21th century. *Global and Planetary Change*, *175*, 226–237.

Palmén, E. (1949). Origin and structure of high-level cyclones south of the: Maximum westerlies. *Tellus*, 1(1), 22–31.

Pinheiro, H. R., Ambrizzi, T., Hodges, K., Gan, M., Andrade, K., & Garcia, J. (2022). Are cut-off lows simulated better in CMIP6 compared to CMIP5? *Climate Dynamics*, *59*(7), 2117–2136.

Pinheiro, H. R., Gan, M., & Hodges, K. (2020). Structure and evolution of intense austral cut-off lows. *Quarterly Journal of the Royal Meteorological Society*, 147(734), 1–20.

Pinheiro, H. R., Hodges, K. I., & Gan, M. A. (2019). Sensitivity of identifying cut-off lows in the southern hemisphere using multiple criteria: Implications for numbers, seasonality and intensity. *Climate Dynamics*, *53*(11), 6699–6713.

Pinheiro, H. R., Hodges, K. I., & Gan, M. A. (2024). Deepening mechanisms of cut-off lows in the southern hemisphere and the role of jet streams: Insights from eddy kinetic energy analysis. *Weather and Climate Dynamics*, *5*(3), 881–894.

Pinheiro, H. R., Hodges, K. I., Gan, M. A., & Ferreira, N. J. (2017). A new perspective of the climatological features of upper-level cut-off lows in the southern hemisphere. *Climate Dynamics*, *48*(1), 541–559.

Pizarro, J., & Montecinos, A. (2000). Cutoff cyclones off the subtropical coast of Chile. In *Proceedings of the 6th International Conference on Southern Hemisphere Meteorology and Oceanography* (pp. 278–279). American Meteorological Society.

Portmann, R., Sprenger, M., & Wernli, H. (2021). The three-dimensional life cycles of potential vorticity cutoffs: A global and selected regional climatologies in ERA-interim (1979–2018). *Weather and Climate Dynamics*, *2*(2), 507–534.

Rahn, D. A. (2014). Observations of the marine boundary layer under a cutoff low over the southeast Pacific Ocean. *Meteorology and Atmospheric Physics*, 123(1–2), 1–15.

Reboita, M. S., Nieto, R., Gimeno, L., Da Rocha, R. P., Ambrizzi, T., Garreaud, R., & Krüger, L. F. (2010). Climatological features of cutoff low systems in the southern hemisphere. *Journal of Geophysical Research D: Atmospheres*, *115*(D17), D17104.

Reboita, M. S., & Veiga, J. A. P. (2017). Análise sinótica e energética de um VCAN que causou chuva no deserto do atacama em março de 2015. *Revista Brasileira De Meteorologia*, *32*, 123–139.

Reinaud, J. N. (2020). Stability of filaments of uniform quasi-geostrophic potential vorticity. *Geophysical & Astrophysical Fluid Dynamics*, *114*(6), 798–820.

Reyers, M., & Shao, Y. (2019). Cutoff lows off the coast of the Atacama Desert under present day conditions and in the last glacial maximum. *Global and Planetary Change_<https://www.sciencedirect.com/journal/global-and-planetary-change>*, 181, 102983.

Rivière, G. (2011). A dynamical interpretation of the poleward shift of the jet streams in global warming scenarios. *Journal of the Atmospheric Sciences*, 68(6), 1253–1272.

Rondanelli, R., Gallardo, L., et al. (2002). Rapid changes in ozone mixing ratios at Cerro Tololo (30° 10 S, 70° 48 W, 2200 m) in connection with cutoff lows and deep troughs. *Journal of Geophysical Research*, 107(D23), 4677.

Rondanelli, R., Hatchett, B., Rutllant, J., Bozkurt, D., & Garreaud, R. (2019). Strongest MJO on record triggers extreme Atacama rainfall and warmth in Antarctica. *Geophysical Research Letters*, *46*(6), 3482–3491.

Vallis, G. K. (2006, November). *Atmospheric and oceanic fluid dynamics: Fundamentals and large-scale circulation*. Cambridge University Press.

Vicuña-Mackenna, B. (1877). Ensayo histórico sobre el clima de chile: (Desde los tiempos prehistóricos hasta el gran temporal de julio de 1877). Imprenta del Mercurio.

Wernli, H., & Sprenger, M. (2007). Identification and ERA-15 climatology of potential vorticity streamers and cutoffs near the extratropical tropopause. *Journal of the Atmospheric Sciences*, *64*(5), 1569–1586.

Wilcox, A., Escauriaza, C., Agredano, R., Mignot, E., Zuazo, V., Otárola, S., Castro, L., Gironás, J., Cienfuegos, R., & Mao, L. (2016). An integrated analysis of the March 2015 Atacama floods. *Geophysical Research Letters*, 43, 8035–8043.